Inorganic Chemistry
Article

Inorg. Chem. **2009**, *48*, 6835–6844 **6835**
DOI: 10.1021/ic900771c

Structure and Physical Properties of New Iron Hydrogenophosphates: $K_2Fe(HP_2O_7)(H_2PO_4)_2$, $LiH_3Fe_2(P_2O_7)_2$, and $FeH_2P_2O_7$

V. Pralong,* R. Baies, V. Caignaert, and B. Raveau

Laboratoire de Crystallographie et Sciences des Matériaux, ENSICAEN, Université de Caen, CNRS, 6 Bd Maréchal Juin, F-14050 Caen 4, France

Received April 21, 2009

The exploration of the systems Fe−H−P−O, Li−Fe−H−P−O, and K−Fe−H−P−O using soft chemistry methods has allowed three new hydrogenophosphates to be synthesized, whose structures have been determined by ab initio calculations. The structures of two of them—$FeH_2P_2O_7$ and $LiH_3Fe(P_2O_7)_2$—exhibit close relationships: their 3D framework consists of $[FeO_4]_\infty$ and $[LiFe_2O_{12}]_\infty$ chains of edge-sharing octahedra, respectively, interconnected through diphosphate groups. These two diphosphates exhibit a paramagnetic to antiferromagnetic transition at low temperatures. The former phase exhibits intrachain ferromagnetic interactions ($\theta_p > 0$) in competition with the antiferromagnetic interchain ordering, whereas for the second one, the ferromagnetic interactions have disappeared due to the presence of Li in the chains. Differently, the third phosphate, $K_2Fe(HP_2O_7)(H_2PO_4)_2$, exhibits a chain structure, involving isolated FeO_6 octahedra, and consequently is paramagnetic in the whole temperature range (4−300 K). Among these three phosphates, only the latter exhibits ionic conductivity, which may originate from the proton mobility.

Introduction

The crystal chemistry of iron phosphates is extremely rich due to the ability of iron to adopt more than one oxidation state, that is, Fe(II) and Fe(III), and to accommodate several coordinations such as octahedral, tetrahedral, or trigonal-bipyramidal. As a result, many Fe(III) phosphates such as $Fe(PO_3)_3$;[1] $LiFeP_2O_7$;[2,3] $FePO_4$;[4] $A_3Fe_2(PO_4)_3$;[5] $Li_9Fe_3(P_2O_7)_3$;[6] and several Fe(II) phosphates such as $NH_4FePO_4 \cdot H_2O$,[7] $Fe_2P_2O_7$,[8] and $SrFe_2(PO_4)_2$[9] have been isolated. Several mixed valent iron oxides have also been synthesized, such as, for example, Fe_2PO_5,[10] $CsFe_3(PO_4)_3 \cdot 2H_2O$,[11] $Fe_3(P_2O_7)_2$,[12] $AFe_5(PO_4)_5(OH) \cdot H_2O$ (A = Ca, Sr),[13] and $NH_4Fe_2(PO_4)_2$.[14] Several of these phosphates exhibit a great potential for various applications, such as, for example, $FePO_4$, which can be used as cathode in lithium ion batteries[15,16,17] or as heterogeneous catalysts for selective oxidation reactions. The magnetic properties of mixed valent iron phosphates were also found interesting in connection with the ordering of Fe^{2+} and Fe^{3+} species and structural transitions.[10−12] Another class of materials that has not been thoroughly explored so far deals with the iron hydrogenophosphates, which represent a potential for the generation of novel structural frameworks, susceptible to exhibiting either protonic conductivity or lithium intercalation, as shown recently for $H_3O[Fe(H_2O)]_3[H_8(PO_4)_6] \cdot 3H_2O$,[18] $Fe_{1.19}PO_4F_{0.11}(OH)_{0.46}(H_2O)_{0.43}$,[19] $Fe_{1.33}(PO_4)$-(OH),[20] and $KFe(H_2P_2O_7)_2$.[21] In most of these hydrogenophosphates,

*To whom correspondence should be addressed. Tel.: +33 2 31 45 26 32. Fax: +33 2 31 95 16 00. E-mail: valerie.pralong@ensicaen.fr.

(1) Elbouaanani, L. K.; Malaman, B.; Gerardin, R. *J. Solid State Chem.* **1999**, *148*, 455.
(2) Riou, D.; Nguyen, N.; Benloucif, R.; Raveau, B. *Mater. Res. Bull.* **1990**, *25*, 1363.
(3) Rousse, G.; Rodriguez-Carvajal, J.; Wurm, C.; Masquelier, C. *Solid State Sci.* **2002**, *4*, 973–978.
(4) Long, G. J.; Cheetham, A. K.; Battle, P. D. *Inorg. Chem.* **1983**, *22*, 3012–3016.
(5) d'Yvoire, F.; Pintard-Screpel, M.; Bretey, E.; de la Rochere, M. *Solid State Ionics* **1983**, *9*, 851.
(6) Poisson, S.; d'Yvoire, F.; Nguyen, H. D.; Bretey, E.; Berthet, P. *J. Solid State Chem.* **1998**, *138*, 32–40.
(7) Greedan, J. E.; Reubenbauer, K.; Birchall, T.; Ehlert, M.; Corbin, D. R.; Subramanian, M. A. *J. Solid State Chem.* **1988**, *77*, 376.
(8) Parada, C.; Perles, J.; Saez-Puche, R.; Ruiz-Valero, C.; Snejko, N. *Chem. Mater.* **2003**, *15*, 3347–3351.
(9) Belik, A.; Azuma, M.; Takano, M.; Lazoryak, B. I. *Chem. Mater.* **2004**, *16*, 4311–4318.
(10) Odaressi, A; Courtois, A.; Gerardin, R.; Malaman, B.; Gleitzer, C. *J. Solid State Chem.* **1981**, *40*, 301–311.
(11) Lii, K.-H.; Huang, C. Y *Inorg. Chem.* **1995**, 571–574.
(12) Ijjaali, M.; Venturini, G.; Gerardin, R.; Malaman, B.; Gleitzer, C. *Eur. J. Solid State Inorg. Chem.* **1991**, *28*, 983–998.
(13) Dvoncova, E.; Lii, K. *Inorg. Chem.* **1993**, *32*, 4368.
(14) Boudin, S.; Lii, K.-H. *Inorg. Chem.* **1998**, *37*, 799–803.
(15) Masquelier, C.; Padhi, A. K.; Nanjundaswamy, K. S.; Goodenough, J. B. *J. Solid State Chem.* **1998**, *135*, 228.
(16) Padhi, A. K.; Nanjundaswamy, K. S.; Goodenough, J. B. *J. Electrochem. Soc.* **1997**, *144*(4), 1188.
(17) Centy, G.; Trifiro, F.; Ebner, J. R.; Franchetti, V. M. *Chem. Rev.* **1988**, *88*, 55–60.
(18) Pralong, V.; Caignaert, V.; Raveau, B. *Solid State Ionics* **2006**, *177*, 2453–2456.
(19) Dollé, M.; Patoux, S.; Richardson, T. J. *J. Power Sources* **2005**, *144*, 208–213.
(20) Song, Y.; Zavalij, P. Y.; Chernova, N. A.; Whittingham, M. S. *Chem. Mater.* **2005**, *17*, 1139–1147.
(21) Chudinova, N. N.; Murashova, E. V.; Ilyukhin, A. B.; Tarnopolskii, V. A.; Yaroslavtsev, A. B. *Inorg. Mater.* **2005**, *41*(1), 69–72.

Published on Web 06/18/2009

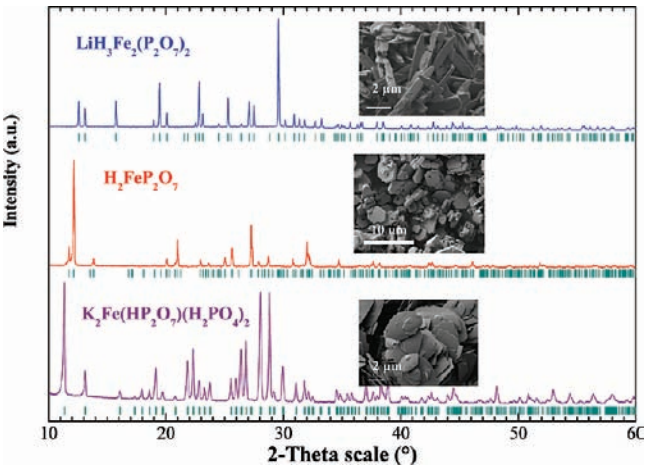

Figure 1. Rietveld refinement plot of X-ray diffraction data for $LiH_3Fe_2(P_2O_7)_2$, $H_2Fe(P_2O_7)$, and $K_2Fe(HP_2O_7)(H_2PO_4)_2$. Inset: SEM image of the phase.

Table 1. Crystallographic Data for $LiH_3Fe_2(P_2O_7)_2$, $H_2Fe(P_2O_7)$, and $K_2Fe(HP_2O_7)(H_2PO_4)_2$

compound	$LiH_3Fe_2(P_2O_7)_2$	$H_2Fe(P_2O_7)$	$K_2Fe(HP_2O_7)(H_2PO_4)_2$
atomic ratio from EDS/AAS	1:2:4	1:2	2:1:4
fw	469.55 g/mol	231.85 g/mol	498.046 g/mol
cryst syst	orthorhombic	monoclinic	orthorhombic
space group	*Pbnb* (56)	$P12_1/c1$ (14)	$Pb2_1a$ (29)
cell params	$a = 13.4850(5)$ Å	$a = 9.2318(2)$ Å	$a = 19.0475(2)$Å
	$b = 9.3502(4)$ Å	$b = 12.7943(2)$ Å	$b = 13.4613(2)$ Å
	$c = 8.2401(3)$ Å	$c = 9.7256(1)$ Å	$c = 5.1012(1)$ Å
		$\beta = 106.81(1)°$	
cell volume	1038.97(7) Å^3	1099.66(2) Å^3	1307.97(3) Å^3
Z	4	8	4
calcd density	3.00 g/cm^3	2.80 g/cm^3	2.55 g/cm^3
χ^2	1.28	2.56	2.32
R_{WP}, R_B	2.18%, 6.61%	1.29%, 8.71%	1.44%, 9.36%

iron exhibits the trivalent state, as shown for the following compounds: $NaBaFe_4(HPO_4)_3 \cdot H_2O$,[22] $NH_4H_8Fe_3(PO_4)_6 \cdot 6H_2O$,[23] $FeH_2P_3O_{10}$,[24] $Fe_4(OH)_3(PO_4)_3$,[25] $Fe(H_2PO_4)_3$,[26] and $Fe(H_3O)(HPO_4)_2$.[27] Very few hydrogenophosphates contain divalent iron. Two examples can be cited: the pure Fe(II) phase $Fe_2(PO_4)(OH)$[28] and the mixed valent iron hydrogenophosphate $Fe_7(HPO_4)(PO_4)_5$.[29] Two mixed valent hydrogenophosphates, $AFe_5(PO_4)_5(OH) \cdot H_2O$,[13] have also been synthesized, with A = Ca and Sr. Bearing in mind these results, we have revisited the synthesis of iron hydrogenophosphates, using soft chemistry methods, that is, starting from Fe_2O_3 or metallic iron dissolved in phosphoric acid, and adding eventually K_2CO_3 or Li_2CO_3 to the solution.

We report, herein, the synthesis, structure, and physical properties of two novel Fe(II) hydrogenophosphates, $LiH_3Fe(P_2O_7)_2$ and $Fe(H_2P_2O_7)$, and one novel Fe(III) hydrogenophosphate, $K_2Fe(HP_2O_7)(H_2PO_4)_2$.

(22) Korzenski, M. B.; Kolis, J. W. *Inorg. Chem.* **2000**, *39*, 5663.
(23) Moore, P. B.; Araki, T. *Am. Mineral.* **1979**, *64*, 587–592.
(24) Lutsko, V.; Johansson, G. *Acta Chem. Scand. A* **1984**, *38*, 663.
(25) Torardi, C. C.; Reiff, W. M.; Takacs, L. *J. Solid State Chem.* **1989**, *82*, 203–215.
(26) Baies, R.; Pralong, V.; Caignaert, V.; Raveau, B. *Mater. Res. Bull.* **2006**, *41*, 1170–1177.
(27) Vencato, I.; Mattievich, E.; Moreira, L. F.; Mascarenhas, Y. P. *Acta Crystallogr., Sect. C* **1989**, *45*, 367–371.
(28) Hatert, F. *Acta Crystallogr., Sect. C* **2007**, *63*(12), i119–i121.
(29) Vencato, I.; de Farias Moreira, L.; Mattievich, E.; Primerano; Mascarenhas, Y. *J. Braz. Chem. Soc.* **1994**, *5*(1), 43–51.

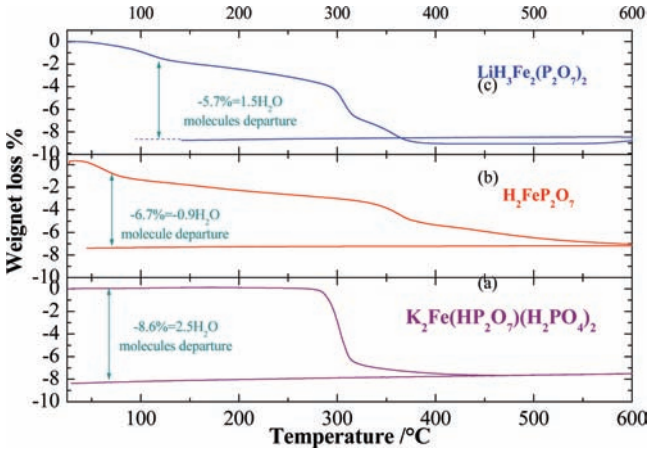

Figure 2. TGA curve under nitrogen flow at 2°/min for $K_2Fe(HP_2O_7)(H_2PO_4)_2$ (a), $H_2Fe(P_2O_7)$ (b), and $LiH_3Fe_2(P_2O_7)_2$ (c).

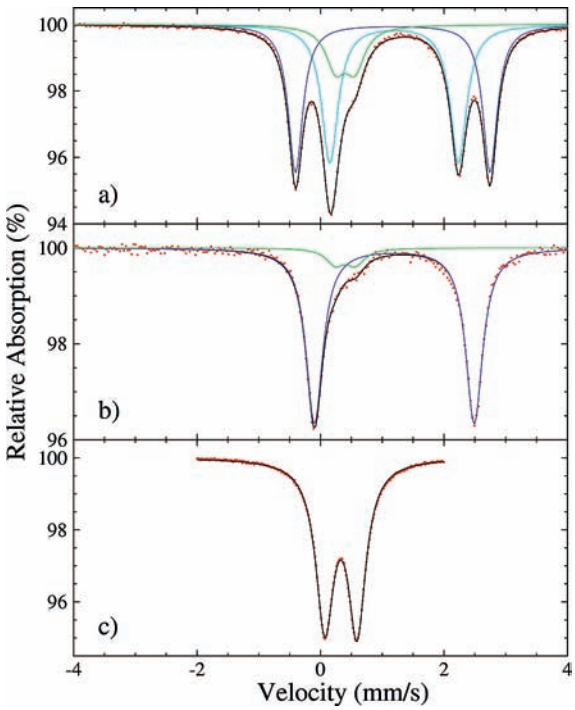

Figure 3. Transmission Mössbauer spectra registered at 298 K for $H_2Fe(P_2O_7)$ (a), $LiH_3Fe_2(P_2O_7)_2$ (b), and $K_2Fe(HP_2O_7)(H_2PO_4)_2$ (c).

Table 2. Isomer Shift (IS) and Quadruple Splitting (QS) for $LiH_3Fe_2(P_2O_7)_2$, $H_2Fe(P_2O_7)$ and $K_2Fe(HP_2O_7)(H_2PO_4)_2$

	IS (mm/s)	QS (mm/s)	Γ (mm/s)	%
$H_2FeP_2O_7$	1.310	2.083	0.16	43.4
	1.287	3.151	0.14	41.2
	0.518	0.314	0.19	15.4
$LiH_3Fe_2(P_2O_7)_2$	1.312	2.588	0.17	91.2
	0.520	0.327	0.18	8.8
$K_2Fe(HP_2O_7)(H_2PO_4)_2$	0.445	0.522	0.17	100.0

Experimental Section

Chemical Synthesis. The synthesis of these three new hydrogenophosphates was carried out in an acidic solution of H_3PO_4

Table 3. Fractional Atomic Coordinates and Isotropic Thermal Factors for (a) $H_2Fe(P_2O_7)$, (b) $LiH_3Fe_2(P_2O_7)_2$, and (c) $K_2Fe(HP_2O_7)(H_2PO_4)_2$

(a) $H_2FeP_2O_7$

atom	Wyck.	*x*/*a*	*y*/*b*	*z*/*c*	*U* [Å^2]
Fe1	4e	0.747(3)	0.255(2)	−0.249(3)	0.016(2)
Fe2	4e	0.746(3)	0.0830(6)	0.008(2)	0.016(2)
P1	4e	0.510(1)	0.2900(9)	−0.063(1)	0.021(9)
O1	4e	0.613(7)	0.215(3)	−0.113(5)	0.027(5)
O2	4e	0.572(8)	0.317(5)	0.094(3)	0.027(5)
O3	4e	0.345(2)	0.249(4)	−0.102(6)	0.027(5)
O4	4e	0.497(4)	0.396(2)	−0.153(3)	0.027(5)
P2	4e	0.549(1)	0.0380(8)	0.229(1)	0.021(9)
O5	4e	0.598(6)	−0.034(4)	−0.106(7)	0.027(5)
O6	4e	0.596(7)	−0.068(2)	0.308(5)	0.027(5)
O7	4e	0.672(4)	0.095(3)	0.185(4)	0.027(5)
P3	4e	0.986(1)	0.2829(9)	0.067(1)	0.021(9)
O8	4e	0.878(6)	0.209(3)	0.110(5)	0.027(5)
O9	4e	0.925(8)	0.183(5)	0.413(3)	0.027(5)
O10	4e	0.137(3)	0.224(4)	0.087(7)	0.027(5)
O11	4e	0.047(3)	0.366(2)	0.195(3)	0.027(5)
P4	4e	0.972(1)	0.4434(8	0.286(1)	0.021(9)
O12	4e	0.113(6)	0.475(4)	0.404(7)	0.027(5)
O13	4e	0.919(7)	0.536(3)	0.184(5)	0.027(5)
O14	4e	0.842(4)	0.111(3)	−0.179(4)	0.027(5)

(b) $LiH_3Fe_2(P_2O_7)_2$

atom	Wyck	*x*/*a*	*y*/*b*	*z*/*c*	*U* [Å^2]
Fe	8e	0.90776(20)	0.4800(4)	0.8616(4)	0.0190(9)
P1	8e	0.7985(3)	0.6696(5)	0.5433(5)	0.0232(9)
O1	8e	0.8727(5)	0.5651(10)	0.6169(14)	0.0232(9)
O2	8e	0.8287(5)	0.7109(12)	0.3643(8)	0.0232(9)
O3	8e	0.6893(4)	0.6286(6)	0.5319(10)	0.0232(9)
O4	8e	0.7996(7)	0.8139(8)	0.6356(12)	0.0232(9)
P2	8e	0.9348(3)	0.2650(5)	0.1988(5)	0.0232(9)
O5	8e	0.9106(8)	0.3234(7)	0.3701(8)	0.0232(9)
O6	8e	0.9684(7)	0.3834(9)	0.0809(11)	0.0232(9)
O7	8e	1.0005(6)	0.1310(8)	0.1992(12)	0.0232(9)
Li	4a	0	0	0	0.0232(9)

(c) $K_2Fe(HP_2O_7)(H_2PO_4)_2$

atom	Wyck.	*x*/*a*	*y*/*b*	*z*/*c*	*U* [Å^2]
K1	4a	0.2696(5)	0.7553(11)	1.0042(12)	0.0151(20)
K2	4a	0.5587(6)	0.5788(10)	0.7848(14)	0.0151(20)
Fe1	4a	0.3648(3)	0.50000	0.9388(10)	0.0013(17)
P1	4a	0.8536(7)	0.3468(11)	0.5445(17)	0.0052(12)
O1	4a	0.9367(13)	0.3548(22)	0.584(4)	0.0162(20)
O2	4a	0.8162(12)	0.4158(23)	0.756(4)	0.0162(20)
O3	4a	0.8299(13)	0.2367(24)	0.608(3)	0.0162(20)
O4	4a	0.8371(12)	0.3770(14)	0.269(2)	0.0162(20)
P2	4a	0.9898(7)	0.3583(9)	0.825(2)	0.0052(12)
O5	4a	0.9813(14)	0.2612(15)	0.985(4)	0.0162(20)
O6	4a	1.0598(13)	0.3890(21)	0.701(5)	0.0162(20)
O7	4a	0.9659(11)	0.4512(21)	0.987(4)	0.0162(20)
P3	4a	0.1975(5)	0.5293(10)	0.7323(17)	0.0052(12)
O8	4a	0.1648(13)	0.4417(13)	0.890(4)	0.0162(20)
O9	4a	0.2031(9)	0.5029(22)	0.435(2)	0.0162(20)
O10	4a	0.1491(13)	0.6222(17)	0.760(3)	0.0162(20)
O11	4a	0.2702(8)	0.5537(20)	0.839(4)	0.0162(20)
P4	4a	0.9066(7)	0.6478(13)	0.580(2)	0.0052(12)
O12	4a	0.9859(15)	0.6693(19)	0.633(4)	0.0162(20)
O13	4a	0.9085(13)	0.5757(17)	0.349(3)	0.0162(20)
O14	4a	0.8699(13)	0.6146(18)	0.837(4)	0.0162(20)
O15	4a	0.8659(2)	0.7453(21)	0.495(4)	0.0162(20)

(85% weight), in ambient atmosphere. For the synthesis of Fe(III) hydrogenophosphates, iron is introduced in the form of Fe_2O_3, and for the synthesis of Fe(II) hydrogenophosphates, iron is introduced in the form of metal or FeO. Such a method allows the presence of any other anionic species than phosphates to be discounted. Thus, for the synthesis of the Fe(III) phase $K_2Fe(H_2PO_4)_2(HP_2O_7)$, a mixture of Fe_2O_3 (1.5 g) and H_3PO_4 (37 mL) was first placed in a borosilicate beaker. Then, after homogenization, K_2CO_3 (10 g) was added, and the mixture was stirred for one day at 200 °C. A white precipitate was obtained, which was washed with water in order to remove the excess phosphoric acid.

For the synthesis of Fe(II) phases $FeH_2P_2O_7$ and $LiFe_2[H_3(P_2O_7)_2]$, a similar experimental method was applied, but using metallic iron instead of Fe_2O_3.

The $FeH_2P_2O_7$ phase was prepared in a borosilicate beaker at 200 °C over two days. A total of 0.5 g of FeO was mixed with 20 mL of H_3PO_4 (85% weight) and stirred. The white powder was washed with pure acetone, filtered, and dried in the air. For $LiH_3Fe(P_2O_7)_2$ synthesis, 2 g of an Fe powder were dissolved in 40 mL of H_3PO_4 and stirred at room temperature. Then, an excess of Li_2CO_3 (7 g) was added, and the mixture was stirred for 2 days at 250 °C. After decanting and dropping the excess of the liquid, the white precipitate was washed with water and filtered. The solid was finally washed with acetone and dried at room temperature.

X-Ray Diffraction and Structure Determination. The X-ray powder diffraction (XRPD) patterns were first collected on a Philips X-Pert diffractometer in order to identify the new phases and to check the purity. Then, pure samples were recorded either on a Philips X-Pert diffractometer, using $K\alpha_{1,2}$ wavelength radiation, or on a Brücker D8 high-resolution spectrometer, using $K\alpha_1$ radiation, in order to carry out structural refinements. The three structures were determined ab initio, from XRPD data using the FOX program,[30,31] based on Monte Carlo methods. The work was done with all default options; hence, the parallel tempering algorithm was used. Previously, a pattern matching was done with the FullProf program[32] for determining cell parameters, peak profile parameters, and diffractometer zero error. The latter parameters were introduced in the FOX program. In order to reduce the degrees of freedom and increase the probability to reach the correct solution, the P and O atoms were introduced as PO_4 tetrahedra in the calculations. Note that the FOX program has the advantage of working on limited data, so that the solution of the structure determination could be found in a first step rapidly on a short scan pattern. The structural refinement was finally carried out with the FullProf program.

Chemical Composition and Morphology. Thermogravimetric analysis (TGA) was performed in a N_2 atmosphere at a heating rate of 2 °C/min with a TG92 Setaram microbalance. The sample morphology was studied with a scanning electron microscope (SEM) XL-30 Philips Field Effect Gun with a resolution of about 1 nm. The cationic composition was checked by energy dispersive spectroscopy (EDS) using a kevex analyzer. Atomic absorption spectroscopy was performed for the titration of the lithium content in the sample $LiH_3Fe(P_2O_7)_2$.

Physical Measurements. The powder Mössbauer resonance spectra were measured at room temperature in transmission geometry by use of a constant acceleration spectrometer and a ^{57}Fe source diffused into a rhodium matrix. The velocity scale was calibrated with a α-Fe foil at room temperature. The spectra were fitted with Lorentzian lines using the unpublished MOSFIT program.[33] The isomer shift values are given with respect to metallic iron at 293 K. The magnetic susceptibility of a powdered sample was measured from 5 to 400 K with a SQUID magnetometer (MPMS, Quantum Design) for an applied field $B = 3000$ Oe. The sample was first zero-field-cooled at 5 K until a stable temperature was reached before applying the magnetic

(30) Cerny, R.; Favre-Nicolin, V. *Powder Diffraction* **2005**, *20*, 359.
(31) Cerny, R.; Favre-Nicolin, V. *J. Appl. Crystallogr.* **2002**, *35*, 734.
(32) Rodriguez-Carvajal, J. *Collected Abstracts of Powder Diffraction Meeting*, Toulouse, France, 1990; Vol. 127
(33) Varret, F. MOSFIT. *Proc. Int. Conf. on the Application of the Mössbauer Effect*, Jaipur, India, 1981; Vol. 129. Teillet, J.; Varret, F. MOSFIT Program, University of Le Mans: Le Mans, France.

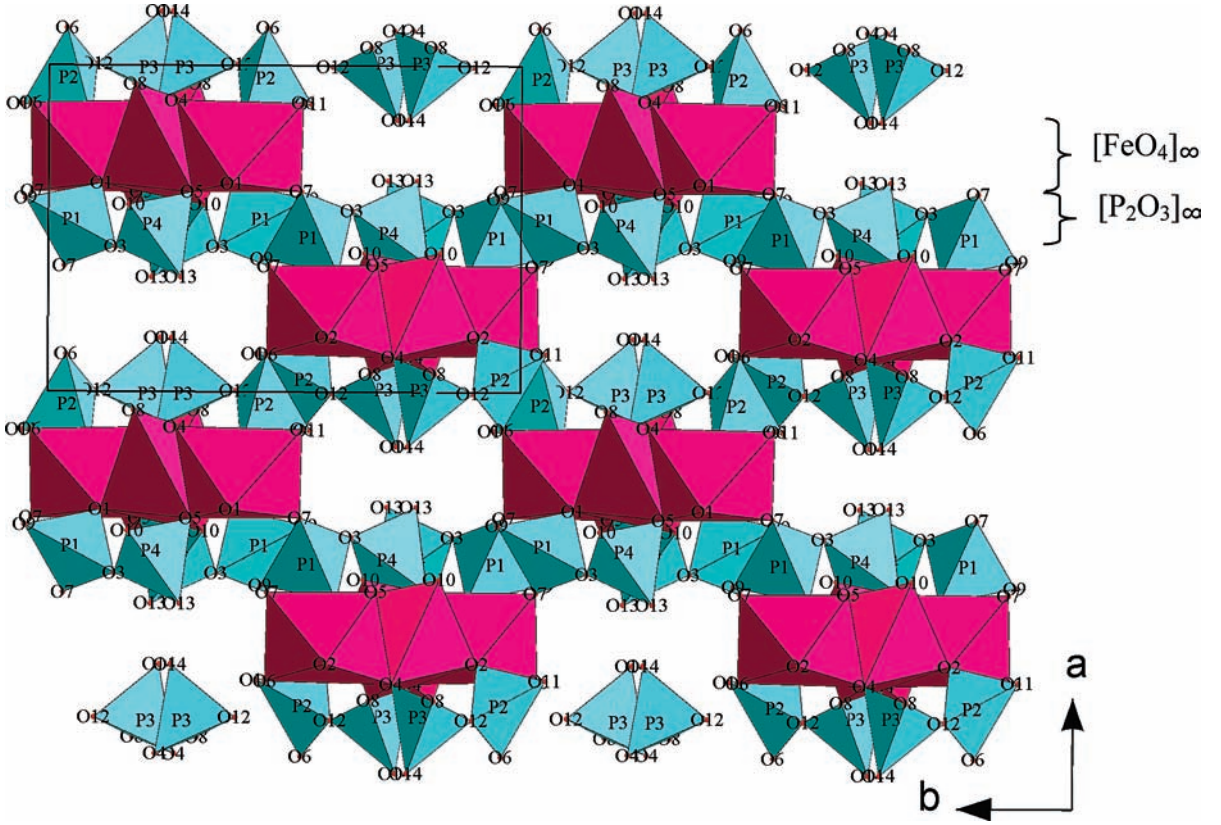

Figure 4. Crystal structure view of $H_2Fe(P_2O_7)$ along the *c* axis.

field. The ^{57}Fe transmission Mössbauer spectra for powder samples were measured at room temperature using a $^{57}Co/Rh$ source. Impedance measurements were carried out with an EG&G 7220 lock-in amplifier in the frequency range 10 Hz to 120 kHz. Pellets were prepared by cold-pressing the powder sample. Gold electrodes were deposited by vacuum evaporation. The impedance measurements were carried out at steady-state temperatures from room temperature to 600 K under an air atmosphere.

Results and Discussion

All of the peaks of the XRPD patterns of the three new phases (Figure 1) were indexed either in an orthorhombic or in a monoclinic cell, attesting their purity. The three compounds show homogeneous shape from SEM analysis with a size comprised between 2 and 5 μm (inset, Figure 1). The cationic composition deduced from EDS measurements (Table 1), combined with atomic adsorption analysis and thermogravimetric analysis carried out under a nitrogen flow (Figure 2), allowed the chemical compositions of these phases to be confirmed: $LiH_3Fe(P_2O_7)_2$, $Fe(H_2P_2O_7)$, and $K_2Fe(HP_2O_7)(H_2PO_4)_2$. The weight loss in $K_2Fe(HP_2O_7)(H_2PO_4)_2$ (Figure 2a) takes place in one step, up to 300 °C, and corresponds exactly to the departure of 2.5 H_2O molecule per formula, leading to the formation of $KFeP_2O_7$ and amorphous phases. Whereas for $FeH_2P_2O_7$ and for $LiH_3Fe(P_2O_7)_2$ (Figure 2b,c) one observes a small weight loss below 100 °C, which corresponds to the departure of adsorbed water due to the hygroscopic nature of these phases, the large weight loss observed up to 335 °C corresponds to the departure of 1.5 H_2O molecule per formula for $LiH_3Fe(P_2O_7)_2$ and ~0.9 H_2O molecule per formula for $FeH_{2-\delta}P_2O_7$. The resulting powder obtained after the heat treatment was amorphous. Due to the large quantity of adsorbed water, the physical properties characterizations are limited. The fact that only 0.9 H_2O molecule is removed for the phase upon heating suggests a partial oxidation of the $FeH_{2-\delta}P_2O_7$, which should be $FeH_{1.8}P_2O_7$. Mössbauer spectroscopy measurements confirm this hypothesis.

Mössbauer Study. The Mössbauer spectra of the as-synthesized compounds registered at room temperature are shown in Figure 3. The Mössbauer spectrum of $FeH_{2-\delta}P_2O_7$ shows three quadrupole doublets. Two doublets, with large isomer shifts, are characteristic of divalent iron in octahedral coordination, while the third doublet corresponds to iron in a trivalent state. In fact, it appears that the sample reacts slowly with the tape used in the sample holder to produce a brown phase. Then, the third doublet originates certainly from the oxidation of the sample (Table 2). The two other quadrupole doublets show that there are two sites for divalent iron in equal proportion in the structure of $FeH_{2-\delta}P_2O_7$.

The Mössbauer spectrum of $LiH_3Fe_2(P_2O_7)_2$ shows only one quadrupole doublet with a large isomer shift and a small trivalent iron contribution. Again, the trivalent iron contribution originates from the oxidation of the sample, and the doublet with a large isomer shift shows that iron is divalent and located on only one octahedral site. In contrast, the Mössbauer spectra of $K_2Fe(HP_2O_7)(H_2PO_4)_2$ can be fitted with a single quadrupole doublet characteristic of trivalent iron. The isomer shift and the quadrupolar splitting indicate that there is only one octahedral site for trivalent iron in the structure of this compound.

Structural Study. The crystal data and details of refinements of the structure of these three compounds are summarized in Table 1. The values of χ^2 and Bragg

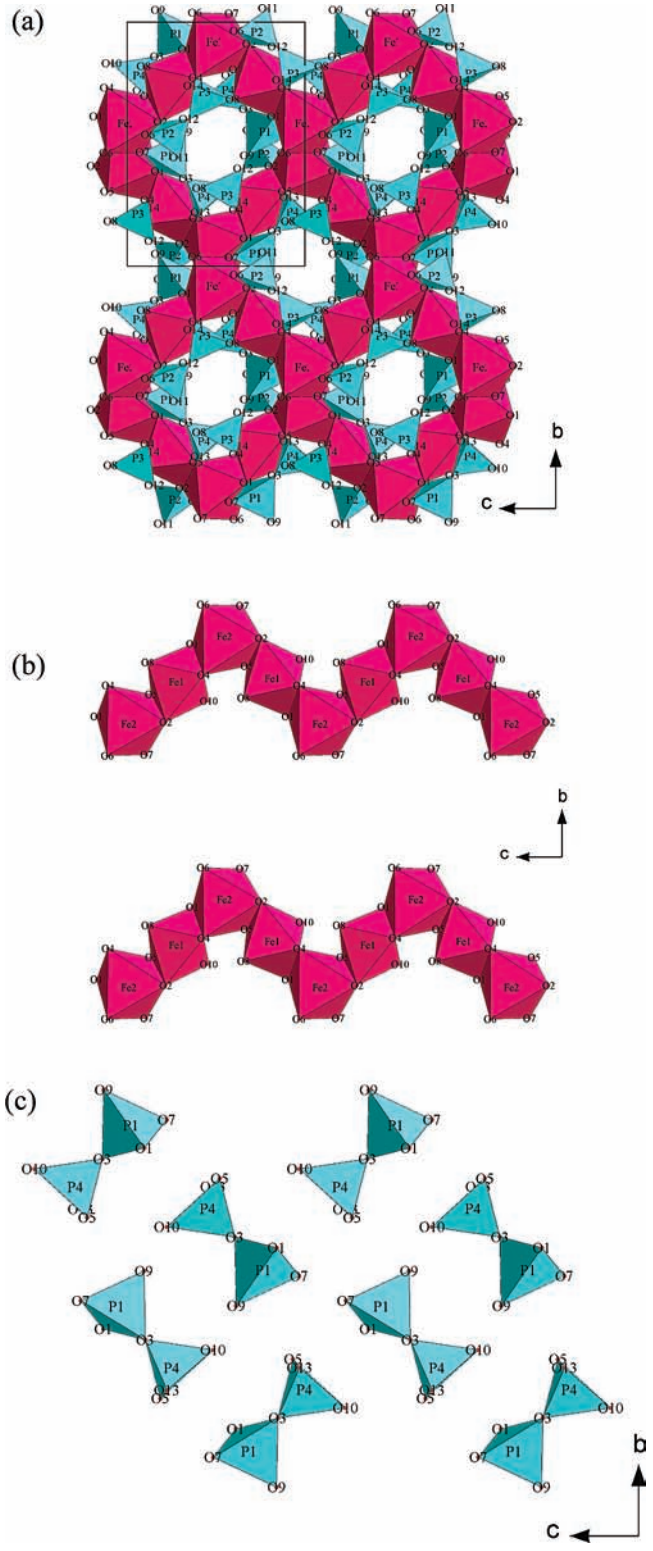

Figure 5. Crystal structure view of $H_2Fe(P_2O_7)$ along the *a* axis (a), (100) $[FeO_4]_\infty$ layer of FeO_6 octahedra forming infinite $[FeO_4]_\infty$ chains of edge-sharing octahedra running along *c* (b), and (100) layer of diphosphate groups forming pairs oriented at 90° (c).

reliability factors show that satisfactory refinement is achieved for the three compounds. The atomic coordinates and isotropic thermal factors are listed in Table 3. Nevertheless, the positions of the hydrogen atoms cannot be determined from such a study and will be discussed later. Note also that no solution could be found in the space group *Pbma* for $K_2H_5FeP_2O_7(PO_4)_2$, and consequently the crystal was determined in the non-centrosymmetric space group $Pb2_1a$.

The structure of $FeH_2P_2O_7$ is similar to that previously determined by Blum et al.[34] for $H_2NiP_2O_7$. It can be described by the stacking along *a* of the $[FeO_4]_\infty$ layers of FeO_6 octahedra interconnected by layers of diphosphate groups (Figure 4). Such $[FeO_4]_\infty$ layers, parallel to (100), consist of isolated $[FeO_4]_\infty$ zigzag chains of edge-sharing octahedra running along *c* (Figure 5a,b). In the diphosphate layers, the diphosphate groups are displayed by pairs oriented at 90° (Figure 5c). Importantly, each phosphate group shares four apexes with the FeO_6 octahedra of two $[FeO_4]_\infty$ chains, belonging to two different layers. Consequently, each diphosphate group has two free apexes, labeled O3, O6, O10, and O13, respectively, for the four independent P atoms of the structure. Note that the free apexes are directed toward the axis of the [001] tunnels formed by the $[FeP_2O_7]_\infty$ framework. The geometry of the polyhedra is in agreement with that generally observed for transition metal phosphates. The interatomic distances are reported in Table 4a. The PO_4 tetrahedra are almost regular with three P−O distances ranging from 1.50 to 1.55 Å, and a longer one comprised between 1.60 and 1.61 Å, corresponding to the bridging oxygen. The Fe−O distances, ranging from 1.97 to 2.18 Å, are close to those expected for Fe(II) oxides.

The structure of $LiH_3Fe(P_2O_7)_2$ is unique (Figures 6 and 7a). It consists of $[LiFe_2O_{12}]_\infty$ layers of LiO_6 and FeO_6 octahedra parallel to (010), interconnected through layers of diphosphate groups (Figure 6). In each $[LiFe_2O_{12}]_\infty$ layer, the octahedra share edges similarly to $FeH_2P_2O_7$ (Figure 4), forming isolated zigzag $[LiFe_2O_{12}]_\infty$ chains running along *c*, but with different periodicity along that direction, since one LiO_6 octahedron alternates with one bioctahedral Fe_2O_{10} unit (Figure 7b). The diphosphate layers exhibit a similar configuration to that observed for $FeH_2P_2O_7$; that is, they are also displayed by pairs oriented at 90° (Figure 7c). Each diphosphate group shares six apexes with the surrounding FeO_6 octahedra, the seventh oxygen atom being the bridging oxygen. Consequently, none of the polyhedra have a free apex, in contrast to $FeH_2P_2O_7$. The PO_4 tetrahedra are rather regular, with three P−O distances ranging from 1.53 to 1.55 Å, and a longer one around 1.59 Å (Table 4b), corresponding to the bridging oxygen. The Fe−O distances, ranging from 2.10 to 2.22 Å, show that the FeO_6 octahedra are rather regular and compatible with the size of the Fe^{2+} cation. The Li−O distances, with four short bonds around 2.05 Å and two longer at 2.31 Å, show that the Li^+ cations sit in elongated octahedra.

Interestingly and unlike $H_2FeP_2O_7$, which shows the same structure as for nickel and cobalt, this iron hydroxyphosphate is not isostructural with the nickel and the cobalt phases. Indeed, the structure of $LiNi_2H_3(P_2O_7)_2$ recently reported[35] is described in the monoclinic space group $C2/c$ with $a = 10.92$ Å, $b = 12.77$ Å, $c = 8.88$ Å, and

(34) Blum, M.; Thauern, H.; Glaum, R. *Phos. Res. Bull.* **2002**, *13*, 83–86.
(35) Yang, T.; Yang, S.; Liao, F.; Lin, J. *J. Solid State Chem.* **2008**, *181*, 1347–1353.

Table 4. Selected Distances and Calculated Valences for (a) $H_2Fe(P_2O_7)$, (b) $LiH_3Fe_2(P_2O_7)_2$, and (c) $K_2Fe(HP_2O_7)(H_2PO_4)_2$

(a) $H_2FeP_2O_7$

bond	length	atom	valence sum calcd
Fe1−O1	2.12(7)	Fe1	2.28(6)
Fe1−O2	2.09(6)	Fe2	2.23(6)
Fe1−O7	2.07(4)	P1	4.88(11)
Fe1−O8	2.12(7)	P2	4.81(12)
Fe1−O9	2.08(6)	P3	4.91(12)
Fe1−O14	2.07(4)	P4	4.93(13)
Fe2−O1	2.16(5)	O1	1.95(9)
Fe2−O5	2.06(5)	O2	1.73(5)
Fe2−O7	2.18(5)	O3	1.21(4)
Fe2−O8	2.14(5)	O4	2.08(6)
Fe2−O12	1.97(5)	O5	1.68(9)
Fe2−O14	2.13(5)	O6	1.19(5)
P1−O1	1.52(6)	O7	2.01(7)
P1−O2	1.51(3)	O8	1.99(10)
P1−O3	1.55(3)	O9	1.76(6)
P1−O4	1.60(3)	O10	1.22(5)
P2−O4	1.60(4)	O11	2.05(5)
P2−O5	1.53(5)	O12	1.83(9)
P2−O6	1.55(4)	O13	1.27(6)
P2−O7	1.52(4)	O14	2.08(7)
P3−O8	1.52(6)		
P3−O9	1.50(4)		
P3−O10	1.54(4)		
P3−O11	1.61(3)		
P4−O11	1.61(3)		
P4−O12	1.52(5)		
P4−O13	1.53(4)		
P4−O14	1.51(4)		

(b) $LiH_3Fe_2(P_2O_7)_2$

bond	length	atom	valence sum calcd
Fe1−O1	2.219(12)	Fe1	1.98(1)
Fe1−O3	2.101(7)	P1	4.88(3)
Fe1−O4	2.130(9)	P2	4.72(4)
Fe1−O6	2.180(10)	O1	1.76(2)
Fe1−O6	2.155(10)	O2	2.14(2)
Fe1−O7	2.097(10)	O3	1.66(2)
P1−O1	1.525(10)		(1.92(2)[a])

Table 4. Continued

(b) $LiH_3Fe_2(P_2O_7)_2$

P1−O2	1.579(9)	O4	1.55(2)
P1−O3	1.524(7)	O5	1.31(4)
P1−O4	1.549(9)		(2.07(4)[a])
P2−O2	1.604(8)	O6	1.85(2)
P2−O5	1.548(8)	O7	1.83(2)
P2−O6	1.541(10)	Li1	1.02(1)
P2−O7	1.534(92)		

(c) $K_2Fe(HP_2O_7)(H_2PO_4)_2$

bond	length/Å	atom	valence sum calcd (exp)
Fe1−O2	2.14(2)	Fe1	2.97(5)
Fe1−O4	2.04(2)	P1	4.74(11)
Fe1−O8	2.07(2)	P2	4.60(11)
Fe1−O12	2.01(2)	P3	4.65(10)
Fe1−O14	1.97(2)	P4	4.68(11)
Fe1−O15	1.92(2)	O1	2.11(6)
P1−O1	1.60(3)	O2	1.56(5)
P1−O2	1.59(3)	O3	1.28(6)
P1−O3	1.58(4)	O4	2.09(7)
P1−O4	1.50(2)	O5	1.33(7)
P2−O1	1.60(2)	O6	1.27(6)
P2−O6	1.55(2)	O7	1.79(6)
P2−O7	1.53(3)	O8	1.28(5)
P2−O8	1.57(3)	O9	1.15(3)
P3−O9	1.56(2)	O10	1.39(6)
P3−O10	1.56(2)	O11	1.96(6)
P3−O11	1.56(3)	O12	1.34(6)
P3−O12	1.52(2)	O13	1.92(6)
P4−O13	1.56(3)	O14	1.99(5)
P4−O14	1.53(2)	O15	1.20(6)
P4−O15	1.55(2)	K1	1.03(2)
P4−O16	1.59(3)	K2	0.96(2)

[a] With H1 (x = 0.878(9), y = 0.268(4), z = 0.427(9)) taken into account for the valence calculation.

$\beta = 123.2°$, and its structure derives from the $H_2MP_2O_7$ (M = Fe, Ni, Co) type structure described above.

The structure of $K_2H_5FeP_2O_7(PO_4)_2$ is also original and very simple. As shown from the projection of the latter along c (Figure 8), it consists of isolated FeO_6

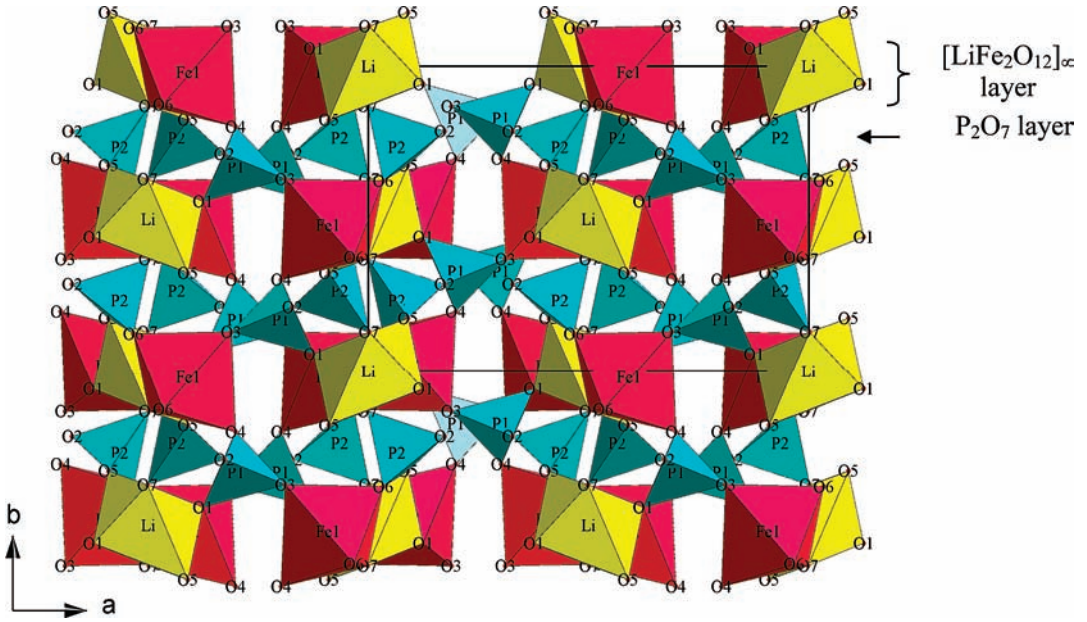

Figure 6. Crystal structure view of $LiH_3Fe_2(P_2O_7)_2$ along the c axis showing the stacking of $[LiFe_2O_{12}]_\infty$ layers of LiO_6 and FeO_6 octahedra with layers of P_2O_7 groups.

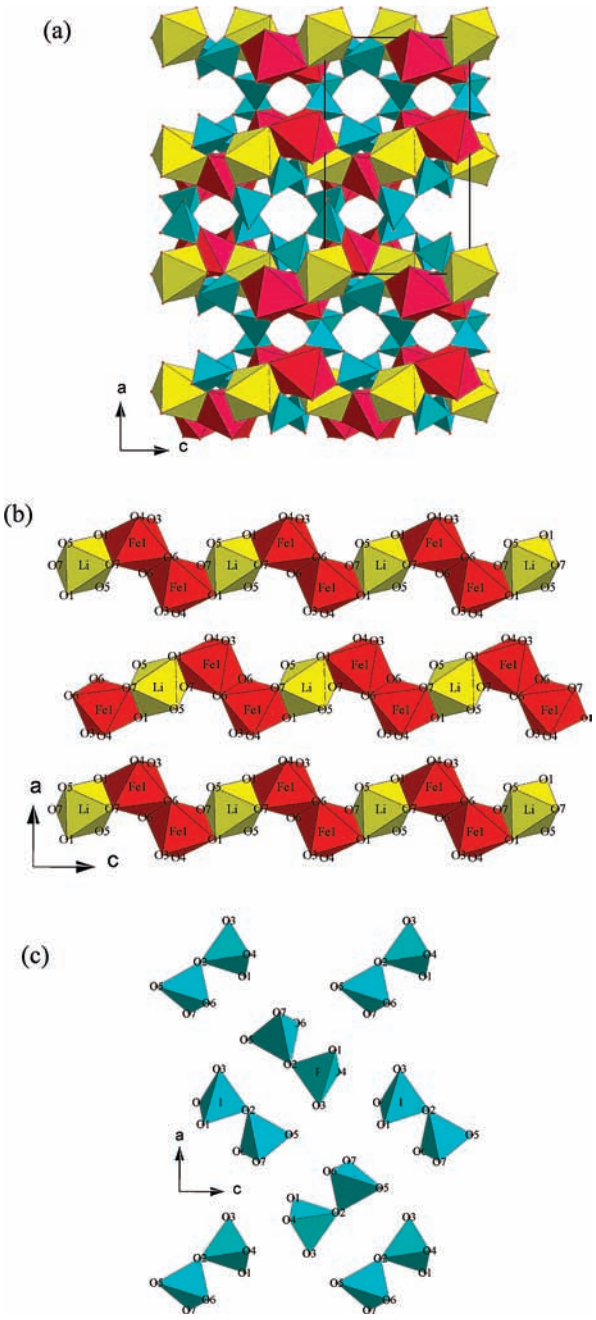

Figure 7. Crystal structure view of $LiH_3Fe_2(P_2O_7)_2$ along the *b* axis (a), $[LiFe_2O_{12}]_\infty$ layers parallel to (010) (b), and (010) layer of diphosphate groups forming pairs oriented at 90° (c).

octahedra only connected to diphosphate and single phosphate groups. In fact, this compound exhibits a chain structure as shown from its projection along *a* (Figure 9). It consists indeed of $[FeP_4O_{15}]_\infty$ chains running along *c*. In each chain, one FeO_6 octahedron shares two apexes with the same diphosphate group, one apex with another diphosphate group, and other apexes with three single PO_4 tetrahedra. Note that only the P_2O_7 groups (P1 and P2) and the P4 tetrahedra ensure the connection between the FeO_6 octahedra along the chain, whereas the P3 tetrahedra share only one apex with one FeO_6 octahedron, the three other apexes being free (Figure 9). Thus, the structure of $K_2H_5FeP_2O_7(PO_4)_2$ can be described as built up of anionic mixed "tetrahedral−octahedral" chains whose cohesion is ensured by the presence of K^+ cations. The interatomic distances are reported in Table 4c.

As already pointed out, the structure calculations give no information about the hydrogen positions. Nevertheless bond valence sum calculations may sometimes bring additional information. The latter were performed according to the Alternatt and Brown method[36] and are listed for each compound in Table 4.

In the case of $FeH_2P_2O_7$, the main valence deficiencies (Table 4a) appear on the O3, O6, O10, and O13, corresponding to the free apexes of the P_2O_7 groups. This result is in perfect agreement with the results and hypothesis previously reported for the isotypic phase $H_2NiP_2O_7$.[37] Thus, the $FeH_2P_2O_7$ structure can be described as being built up of $P_2O_5(OH)_2$ groups with H atoms localized in the [001] tunnels (Figure 3) and between the diphosphate groups, reinforcing the cohesion of the structure of this hydrogenophosphate Fe-$[P_2O_5(OH)_2]$.

For $LiH_3Fe_2(P_2O_7)_2$, the valence deficiency (Table 4b) appears mainly on four oxygen sites—O1, O3, O4, and O5—but the difference is not so obvious between these different sites. Additionally, in this structure, there is no free apex for the P_2O_7 and FeO_6 polyhedra. The geometry of the diphosphate layers (Figure 7c) is rather similar to that observed for $FeH_2P_2O_7$ (Figure 5) and suggests that the H atoms are mainly localized between these diphosphate groups. The unit cell should contain 12 hydrogen atoms that should then be distributed either on one general Wyckoff site (8e) and a special Wyckoff site (4b, 4c, or 4e), or on two general Wyckoff sites, with at least one site partially occupied. Otherwise, one hydrogen atom located at 0.82 Å from an oxygen atom brings a contribution of about 0.77 to the oxygen valence. O5 is then the only oxygen site that can form a bond with a fully occupied hydrogen site to have a valence close to that expected. Furthermore, this hydrogen can form a hydrogen bond with the O3 site, increasing the valence of this oxygen atom. A fully occupied hydrogen site at $x = 0.878$, $y = 0.268$, and $z = 0.427$ leads to correct distances and proper valences for the O5 and O3 atoms by forming O−H···O hydrogen bonds. The four remaining hydrogen atoms should be localized at random near the O4 site.

In the case of $K_2H_5FeP_2O_7(PO_4)_2$, valence deficits (Table 4c) appear clearly on five oxygen sites out of 15, that is, on O6, O9, O10, O12, and O15. All of these atoms correspond to free apexes either of the P_2O_7 groups (O6) or of the PO_4 groups (O9, O10, O12, and O15). Thus, the structure can be described as being built up of $P_2O_6(OH)$ groups and $PO_2(OH)_2$ tetrahedra, leading to the formulation $K_2Fe[P_2O_6(OH)][PO_2(OH)_2]_2$. Thus, the cohesion of the structure of this phase is ensured by both ionic bonds between the anionic chains $[H_5FeP_4O_{15}]_n^{2n-}$ and K^+ cations and by O−H···O hydrogen bonds between these chains.

(36) Brown, I D; Alternatt, D *Acta Crystallogr.* **1985**, *B41*, 244.
(37) Yang, T.; Ju, J.; Li, G.; Yang, S.; Sun, J.; Liao, F.; Lin, J.; Sasaki, J.; Toyota, N. *Inorg. Chem.* **2007**, *46*, 2342–2344.
(38) Torardi, C. C.; Reiff, W. M.; Takacs, L. *J. Solid State Chem.* **1989**, *82*, 203–215.
(39) Song, Y.; Zavalij, P. Y.; Suzuki, M.; Whittingham, M. S. *Inorg. Chem.* **2002**, *41*(22), 5778.
(40) Kittel, C. *Solid State Physics*; J. Wiley and Sons Inc.: New York, 1956.

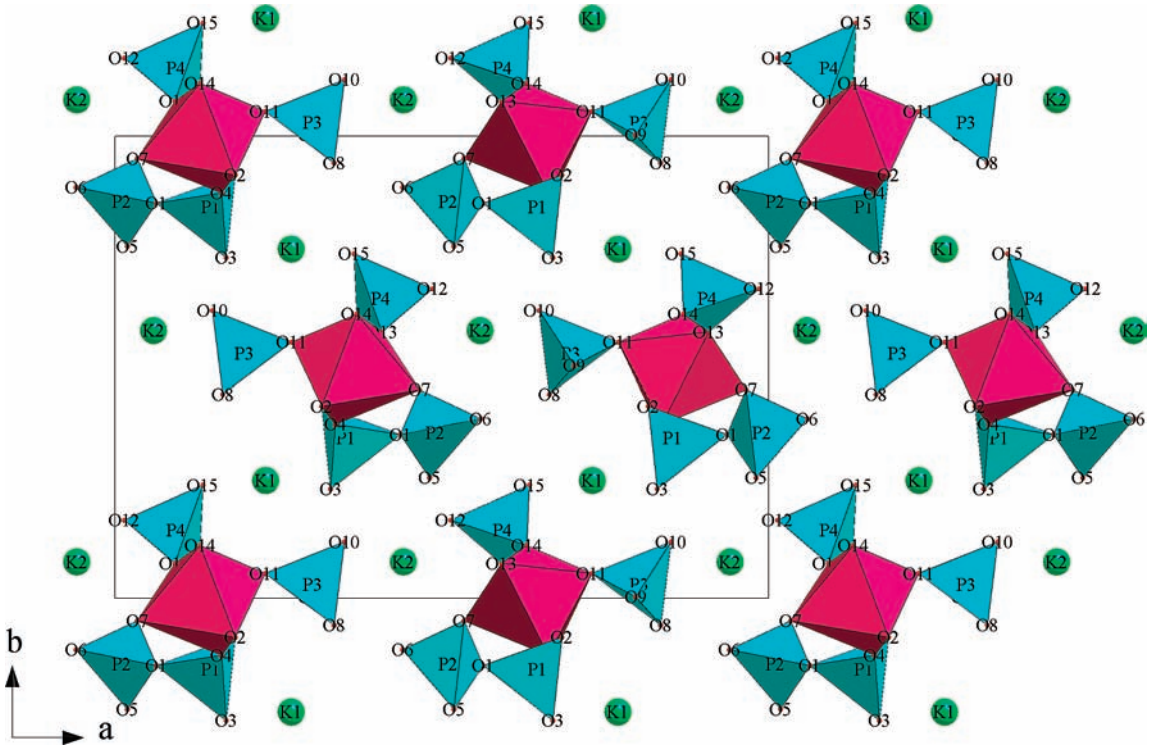

Figure 8. Crystal structure view of $K_2Fe(HP_2O_7)(H_2PO_4)_2$ along the *c* axis.

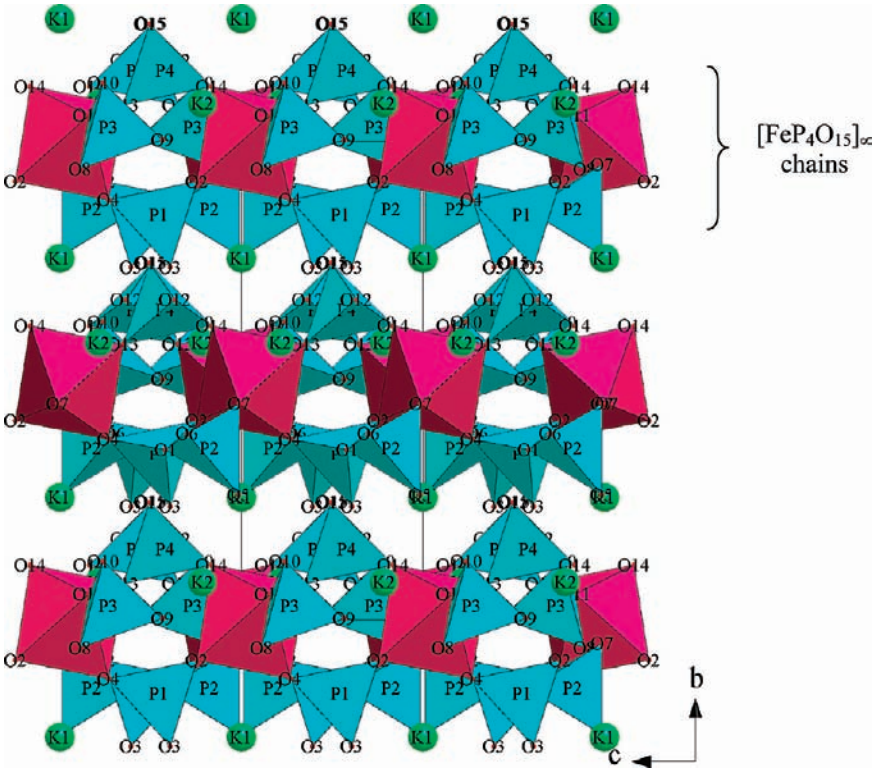

Figure 9. Crystal structure view of $K_2Fe(HP_2O_7)(H_2PO_4)_2$ along the *a* axis, showing the $[Fe(PO_4)_2P_2O_7]_\infty$ chains running along *c*.

Magnetic Properties. The magnetic susceptibility curves $\chi(T)$ and $\chi^{-1}(T)$, both zero-field-cooled (ZFC) and field-cooled (FC) for the three compounds, are plotted in Figure 10. For these three samples, the data registered above 20 K can be fitted with the Curie−Weiss law: $\chi_M = \chi_0 + \frac{C_m}{T-\theta_P}$ showing that, in this temperature range, they exhibit paramagnetic behavior. The effective magnetic moments μ_{eff} per Fe, $\mu_{eff} = \mu/\mu_B$ with $\mu = \sqrt{[(3k_BC_m)/N_A]}$ (with k_B being the Boltzmann constant and N_A Avogadro's number), deduced from these curves (Table 5) are in quite good agreement with the expected ones for Fe^{3+} and Fe^{2+} in the high-spin ground state. Both $FeH_2P_2O_7$

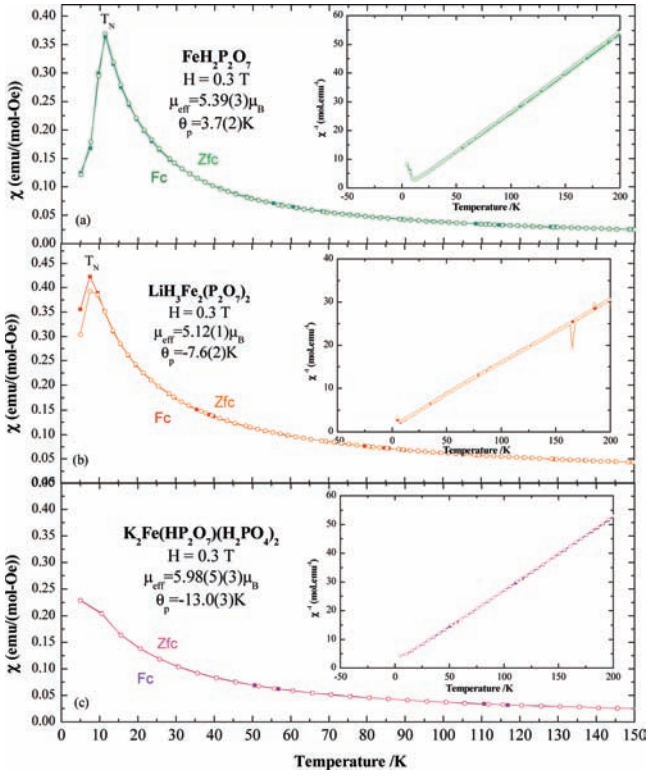

Figure 10. Susceptibility versus temperature $\chi(T)$ for $LiH_3Fe_2(P_2O_7)_2$, $H_2Fe(P_2O_7)$, and $K_2Fe(HP_2O_7)(H_2PO_4)_2$. Inset: corresponding $\chi^{-1}(T)$ curves.

(Figure 10a) and $LiH_3Fe_2(P_2O_7)_2$ (Figure 10b) show a very narrow peak at $T_N = 11.0$ K and $T_N = 7.5$ K, respectively, with superposition of the ZFC and FC curves, that is, characteristic of a transition from the paramagnetic to the antiferromagnetic (AFM) state as T decreases below these temperatures.

The sharp increase of χ as T decreases from 50 K to T_N and the positive value of $\theta_p = 3.7$K for $H_2FeP_2O_7$, together with the decrease of χ below T_N, suggest that this phase exhibits short-range FM interactions below T_N in competition with the AFM long-range ordering of the matrix. Bearing in mind that such a structure consists of $[FeO_4]_\infty$ chains of edge-sharing FeO_6 octahedra, it is most likely that the FM coupling appears along the chains, whereas the AFM ordering is due to the AFM coupled between the chains. In contrast, $LiH_3FeP_2O_7$ is characterized by a negative θ_p value of -7.6 K, showing that the FM interactions along $[LiFe_2O_{12}]_\infty$ chains do not exist, due to the fact that the LiO_6 octahedra displayed between the Fe_2O_{10} bioctahedral units break such interactions.

No transition could be detected for $K_2FeH_5P_4O_{15}$ (Figure 10c) down to 5 K, and the compound remains paramagnetic down to 5 K, in agreement with the fact that the FeO_6 octahedra are isolated.

Ionic Conduction Properties. The presence of protons and lithium or potassium cations in the three phosphates raises the issue of protonic or ionic conductivity. The compounds $FeH_2P_2O_7$ and $LiH_3Fe_2P_2O_7$ do not show any signature of such conductivity. In contrast, the compound $K_2FeH_5P_4O_{15}$ is of interest. The impedance plots were obtained for this phase, between 10 Hz and 120 kHz under air. The compound was studied between

Table 5. Magnetic Properties of the Samples Calculated from the DC Magnetisation Data[a]

	μ_{eff}/μ_B	θ_p/K	ref
$LiH_3Fe_2(P_2O_7)_2$ (Fe^{2+})	5.12(1)	−7.6(1)	this work
$FeH_2P_2O_7$ (Fe^{2+})	5.39(3)	3.7(2)	this work
$K_2Fe(HP_2O_7)(H_2PO_4)_2$ (Fe^{3+})	5.98(5)	−13.0(3)	this work
$Fe(H_2PO_4)_3$ (Fe^{3+})	6.08	−42.7(4)	26
$Fe_{1.18}(PO_4)(OH)_{0.57}(H_2O)_{0.43}$	4−4.5		37
$Fe_4(OH)_3(PO_4)_3$	4.2	86.6 + 0.3	38
$FePO_4$ 2H_2O monoclinic	6.392	−179.8	39
$FePO_4$ 2H_2O orthorhombic	6.305	−120.1	39
$Fe^{2+}(d^6)$ high spin in octahedral site	*4.90*		40
Fe^{3+} (d^5) high spin in octahedral site	*5.92*		40

[a] θ_p is the Curie−Weiss temperature. μ_{eff} is the effective paramagnetic moment calculated in the paramagnetic regime of M−T data.

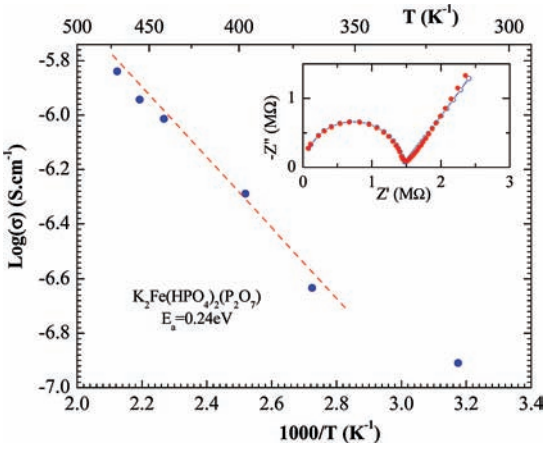

Figure 11. Arrhenius plot $\log(\sigma)$ versus 1000/T of $K_2Fe(HP_2O_7)$-$(H_2PO_4)_2$. Inset: Nyquist plot at room temperature.

room temperature and 250 °C, due to its poor thermal stability. A semicircle is observed at high frequencies, followed by a spike in the low-frequency region (inset, Figure 11). The conductivity increases with temperature, reaching $10^{-5.7}$ S/cm at 500 °C (470 K). The plot of $\log(\sigma)$ versus $1/T$ (Figure 11) exhibits a linear behavior, characteristic of the classical Arrhenius relation. It evidences only one regime of conductivity characterized by an activation energy $E_a = 0.24$ eV. These results clearly establish that this hydrogenophosphate is an ionic conductor. It is of course not possible to distinguish between K^+ or H^+ ion transport nor to detect which hydrogen atoms are responsible for the conduction and then to determine the exact nature of the conductivity, that is, to distinguish surface conductivity from bulk conductivity. Nevertheless, it is worth pointing out that the same order of magnitude of ionic conductivity was obtained for the protonic conductor $H_3OFe(H_2O)_3[H_8(PO_4)_6]\cdot 3H_2O$,[18] whose ionic conduction reaches 10^{-5} S/cm at 300 K. Similarly, the phase $KFe(H_2P_2O_7)_2$,[21] which also contains protons, exhibits a conductivity $\sigma = 3.10^{-6}$ S/cm in the temperature range 370−550 K ($E_a = 0.59$ eV).

Conclusions

In the present work, we have demonstrated the great potential of iron hydrogenophosphate systems for the generation of new frameworks, combining soft chemistry methods for the synthesis and ab initio calculations for the

structure determination. From the viewpoint of magnetic properties, the phosphates $FeH_2P_2O_7$ and $LiH_3Fe(P_2O_7)_2$ attract particular interest due to the fact that their structure consists of isolated octahedral zigzag chains, suggesting quasi-unidimensional magnetic interactions for the former and more magnetic clusters at the level of Fe_2O_{10} bioctahedra for the second one. Such magnetic behavior should be studied more in detail in the future. In contrast, the phosphate $K_2Fe\text{-}[P_2O_6(OH)][PO_2(OH)_2]_2$, which shows isolated FeO_6 octahedra, is simply paramagnetic, but the evidence for ionic conductivity in this phase, probably due to protons, suggests that investigation of such a property in the family of hydrogenophosphates should be encouraged.

Acknowledgment. The authors want to thank S. Rey for technical help. They gratefully acknowledge the CNRS and European Union through the Novelox program, the network of excellence FAME.